RESEARCH *New Phytol.* (2000), **148**, 481–491

Pseudothecia of Swiss needle cast fungus, *Phaeocryptopus gaeumannii*, physically block stomata of Douglas fir, reducing CO_2 assimilation

DANIEL K. MANTER[1], BARBARA J. BOND[1], KATHLEEN L. KAVANAGH[2], PABLO H. ROSSO[3] AND GREGORY M. FILIP[1]*

[1] *Department of Forest Science, Oregon State University, Corvallis, OR 97331, USA*
[2] *Department of Forest Resources, University of Idaho, Moscow, ID 83844, USA*
[3] *Department of Botany and Plant Pathology, Oregon State University, Corvallis, OR 97331, USA*

Received 17 January 2000; accepted 4 August 2000

SUMMARY

The following study investigates the timing and mechanism of impact of Swiss needle cast on Douglas-fir (*Pseudotsuga menziesii*) needle physiology (i.e. gas exchange). Swiss needle cast is a foliar disease caused by the fungus *Phaeocryptopus gaeumannii*, which occurs throughout the range of Douglas fir and until recently has been considered unimportant. However, recent surveys show the Swiss needle cast currently affects >52611 ha of forested lands in western Oregon, USA, causing a reduction in growth of *c.* 23% or an implied growth loss of *c.* 3.2 m^3 ha^{-1} yr^{-1} for 1996 alone. Gas exchange of artificially inoculated 2-yr-old Douglas-fir seedlings was monitored on a monthly basis using A/C_i curve analysis. No effect of fungal presence on gas exchange was noted until the emergence of fungal fruiting structures (pseudothecia) from needle stomata. However, once present, maximum stomatal conductance and CO_2 assimilation rates were inversely proportional to the presence of pseudothecia. A/C_i curve analysis showed that declines in CO_2 assimilation appeared to be due to both stomatal and nonstomatal limitations. Stomatal limitations to CO_2 assimilation were the direct result of reduced CO_2 diffusion through blocked stomata. Nonstomatal limitations arose, in part, from an indirect effect of pseudothecia development on Rubisco activation. For example, in both Swiss needle cast-infected foliage and foliage with artificially blocked stomata (by external application of petroleum jelly), the amount of Rubisco activation showed a strong, positive relationship with daily maximum stomatal conductance. A mechanism is proposed that outlines the impact of pseudothecia development on stomatal conductance and CO_2 assimilation rates.

Keywords: *Pseudotsuga menziesii*, *Phaeocryptopus gaeumannii*, pathogenic fungi, gas exchange, stomatal conductance, photosynthesis, Rubisco activation, seasonal variation.

INTRODUCTION

Swiss needle cast (SNC) is a foliar disease caused by the fungus *Phaeocryptopus gaeumannii*, which occurs throughout the range of Douglas fir (*Pseudotsuga menziesii*) and until recently has been considered unimportant. However, recent surveys show that SNC currently affects >52611 ha of forested lands in western Oregon, USA (Hansen *et al.*, 2000), causing a reduction in growth of *c.* 23% or an implied growth loss of *c.* 3.2 m^3 ha^{-1} yr^{-1} for 1996 alone (D. A. Maguire, unpublished).

*Author for correspondence (tel +1 541 737–6567; fax +1 541 737–1393; e-mail Greg.Filip@orst.edu).

Parasitic fungi extract the nutrients necessary for their survival from the plant tissues that they invade, consequently reducing host growth and vigour. In addition to direct absorption of nutrients, fungi might also reduce host photosynthate production (Šutić & Sinclair, 1991; Scholes, 1992) through a variety of biochemical and/or structural means. Biochemical processes include changes in host processes (e.g. electron transfer chain, Montalbini *et al.*, 1981) and enzymes (e.g. Rubisco, Gordon & Duniway, 1982; Walters & Ayres, 1984) or the introduction of fungal enzymes, which regulate host physiology abnormally (e.g. invertase, Tang *et al.*, 1992). Structural means include the loss of functional

host tissue (e.g. necrosis) and physical blocking of intercellular spaces or stomata (Ayres, 1976, 1981; Šutić & Sinclair, 1991). The latter has been suggested to be the major initial impact of *P. gaeumannii* owing to the presence of fungal fruiting bodies (pseudothecia) that emerge from needle stomata.

The hypothesis that *P. gaeumannii* has an effect on gas exchange of Douglas-fir needles mainly through blockage of stomata is largely based on circumstantial evidence. For example, microscopic work has shown that internal colonization by *P. gaeumannii* is limited to intercellular spaces with no obvious development of haustoria, penetration or necrosis of needle tissue (Capitano, 1999), and pseudothecia initials can be observed densely packed into needle stomata (Stone & Carroll, 1986). Based on these observations and preliminary field data (D. K. Manter, unpublished) showing reduced gas exchange in Douglas-fir stands infected with *P. gaeumannii*, we conducted the following studies in order to quantify the effects of *P. gaeumannii* infection on Douglas-fir needle physiology, especially the factors controlling CO_2 assimilation rates, and to determine the mechanism of effect.

MATERIALS AND METHODS

Plant material and inoculations

All measurements were conducted on potted 2-yr-old Douglas fir (*Pseudotsuga menziesii* (Mirb.) Franco) seedlings (Georgia-Pacific Corp., Cottage Grove, OR, USA). In May 1998, 50 seedlings were inoculated by placing seedlings in a chamber with an overhead misting system. Mist was applied for 15 s every 60 min from 08:00 to 20:00 hours, and 15 s every 120 min from 20:00 to 08:00 hours. An inoculum source was provided by branches infected with *Phaeocryptopus gaeumannii* (Rhode) Petrak, collected from Sour Grass Summit, OR, USA, suspended over the target seedlings. Inoculum levels were monitored by weekly spore counts on glass slides suspended over the target seedlings (*c.* 1 spore mm^{-2}). After a 2-wk inoculation period, seedlings were incubated for 2 wk in a glasshouse maintained at 21°C under ambient light and humidity. Immediately following the incubation period, a second round of inoculation (using newly collected inoculum-source branches) and incubation treatments were applied. Following treatments, seedlings were maintained in an outdoor cold frame at Oregon State University, Corvallis until future measurements. For each step of the inoculation procedure (i.e. inoculation, incubation and storage), seedling position was varied randomly. To create noninfected control branches, two branches on each seedling were covered with bags ('D'-bag w/polypropylene window; Northwest Mycological Consultants, Corvallis, OR, USA) during the inoculation and incubation periods. The bagging of branches was successful in reducing overall infection; however, some infection was eventually detected.

Fungal infection

The presence of *P. gaeumannii* was determined by visual estimates of fungal fruiting bodies (pseudothecia) emerging from stomata. Estimates of the percentage of needle stomata that were occluded with pseudothecia (i.e. pseudothecia counts) for each branch were calculated by averaging pseudothecia counts from three positions on each needle present. At each position, one on each longitudinal third of the needle, pseudothecia counts were conducted by visually counting the number of pseudothecia emerging from 100 consecutive stomata from the first complete row closest to the needle midrib.

Gas-exchange measurements

Using a LI-COR 6400 portable infrared gas-exchange system (LI-COR, Lincoln, NE, USA), response curves of CO_2 assimilation (A/C_i response curve, i.e. CO_2 assimilation rate vs calculated internal CO_2 concentration) were measured. During measurements, cuvette conditions were maintained at PAR 2000 μmol m^{-2} s^{-1}, temperature 25°C, [H_2O vapor] $\geqslant$18 mmol mol^{-1} air, [CO_2] 40 Pa, and flow rate 100 μmol m^{-2} s^{-1}, unless otherwise stated. A/C_i response curves were measured by varying the cuvette CO_2 concentration, allowing equilibration to a steady state (cuvette [CO_2] coefficient of variation $<2\%$), and logging measurements every 10 s for 1 min. CO_2 was varied as follows: 40, 30, 20, 60, 80, 100, 120, 160 and 200 Pa.

Temporal variation in gas exchange was measured each month from October 1998 to June 1999 using one bagged (i.e. control) and one unbagged (i.e. infected) 1-yr-old branch from at least two seedlings, except for March (six seedlings), April and May (five seedlings); sample sizes were increased in March because of increased variation associated with the development of *P. gaeumannii*-pseudothecia. Beginning in March, low levels of infection (pseudothecia) were observed in most infected branches and some control branches. As a result, control-branch needles were preferentially selected based on the absence of pseudothecia, and infected-branch needles were selected based on the presence of pseudothecia.

A/C_i curves were used to estimate some of the major limitations to net uptake of carbon (C) into a plant following methods described by Farquhar *et al.* (1980), Sharkey (1985), Harley & Sharkey (1991) and Harley *et al.*, (1992). All A/C_i curve calculations are in Appendix I, and a list of abbreviations and parameters can be found in Appendix II.

Imaging chlorophyll fluorescence

In April 1999, needles (1998 cohort) from the six seedlings selected for the April A/C_i curve analysis was also analysed for chlorophyll fluorescence. Following gas exchange, sample branches (one infected and one control branch per seedling) were removed, re-cut under water, and then dark-adapted for 1 h. After the dark treatment, four or five needles were removed from each branch, cut longitudinally in half, and placed side by side on index cards creating two samples per branch (i.e. one sample with four or five needle-tip halves, and one with four or five needle-petiole halves). For each card, a 1-cm^2 sample was measured for chlorophyll fluorescence. For each 1-cm^2 sample, a two-dimensional image of fluorescence was created using an imaging fluorometer that measures time-dependent fluorescence from an array of 31 680 positions per sample. A description of the imaging fluorometer used can found in Ning *et al.* (1995).

For each position, an estimate of quantum yield (Y') was calculated from measurements of F_m (the maximum fluorescence signal), F_s (the low, steady-state level of fluorescence 105 s after illumination) and F_{dark} (the background level of fluorescence); where $Y' = (F_m - F_s)/(F_m - F_{dark})$. A more detailed explanation of the parameters and Eqns can be found in Ning *et al.* (1995) and Bowyer *et al.* (1998).

Rubisco activation

In order to confirm A/C_i estimates of Rubisco activation (i.e. V_{cmax}, see Appendix I), spectrophotometric assays of initial and total Rubisco activity (R_I and R_T, respectively) were measured from a random sample of 10 seedlings. From each seedling, two samples (one infected and one control branch) of six needles (1998 cohort) were analysed and the percentage of activated Rubisco (i.e. Rubisco activation, R_{ACT}) was calculated as $R_I/R_T \times 100$. Needles were homogenized in 3 ml of extraction buffer (100 mM Bicene, 5 mM EDTA, 0.75% (w/w) polyethylene glycol, 14 mM ß-mercaptoethanol and 1% (v/v) Tween 80, pH adjusted to 7.8 using 2N KOH). The extract was centrifuged at 13 000 ***g*** for 40 s, and 50 µl of the supernatant was added to each of two samples of 900 µl of analysis buffer (100 mM Bicene (pH 8.0 at 25°C), 25 mM $KHCO_3$, 20 mM $MgCl_2$, 3.5 mM ATP, 5 mM phosphocreatine, 80 nkat glyderaldehyde-3-phosphate dehydrogenase, 80 nkat 3-phosphoglyceric phosphokinase, 80 nkat creatine phosphokinase and 0.25 mM NADH). For initial Rubisco activity, 50 µl RuBP was immediately added to one sample of the analysis buffer (total preparation time was *c.* <2 min) and changes in A_{340} were measured 15 s later, when a steady slope was observed. For total (fully activated) Rubisco activity, RuBP was added after 15 min of activation and changes in A_{340} were measured.

In order to test the hypothesis that reduced stomatal conductance causes a decline in Rubisco activation, we also measured Rubisco activation on needles that were artificially induced to have lower stomatal conductance. To achieve this we covered the abaxial surface of selected needles (using only 1999 needles with no visible pseudothecia) with one of three different amounts of petroleum jelly (0, 50 and 100% of projected leaf area). Each treatment level was applied to one secondary lateral branch on each of six randomly selected seedlings. Pre- (<30 min) and post- (*c.* 1 h) treatment stomatal conductance was measured using a LI-COR 6200 under natural conditions. Initial and total Rubisco activity were measured 1 d after treatment on needles exposed to full sunlight.

Statistical analysis

All reported values are the means for each measured branch. Within each sample date, differences in gas-exchange parameters and fungal infection (pseudothecia density) between infected and noninfected branches were tested using a paired *t*-test (n = number of seedlings; see the *Gas-exchange measurements* section). All linear regressions were calculated using Sigma Plot 4.0 (Jandel Scientific, San Rafael, CA, USA).

RESULTS

Seasonal variation

The rate of net CO_2 assimilation differed seasonally in both infected and control branches (Fig. 1a). Net assimilation declined by *c.* 40% between December and January, associated with a reduction in stomatal conductance of *c.* 60% (Fig. 1b). Assimilation rates remained constant at these reduced levels until March and the onset of budbreak. In March, assimilation declined a further *c.* 20% for both infected and control branches. At this time, respiration rates also increased *c.* 50% (e.g. R_{day} *c.* 4 µmol CO_2 m^{-2} s^{-1} (Mar) and *c.* 2 µmol CO_2 m^{-2} s^{-1} (Oct-Feb); Fig. 1c). By June, assimilation rates of control branches recovered to 87% of pre-winter rates and conductance of *c.* 80%. In infected branches, however, no recovery in assimilation rates and conductance was observed; in fact, assimilation and conductance were at their lowest observed values (i.e. 26 and 15% of the pre-winter values, respectively).

Seasonal changes in Rubisco activation (V_{cmax}) mirrored changes in stomatal conductance (Figs 1b, 2a). V_{cmax} declined *c.* 22% between December and January (Fig. 2a) compared with the 60% decline in stomatal conductance (Fig. 1b). V_{cmax} remained depressed during the winter until recovery in the

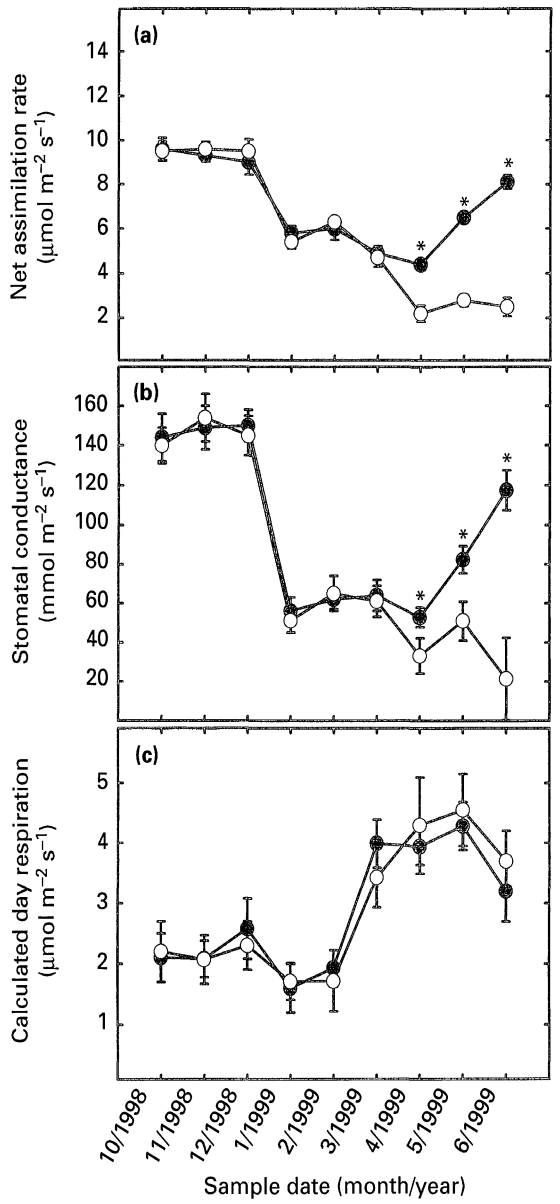

Fig. 1. Seasonal patterns of needle physiology (gas exchange) in 2-yr-old Douglas-fir seedlings infected with *Phaeocryptopus gaeumannii* (open circles, infected; closed circles, control). For each sample date, treatment differences were tested using a paired *t*-test; *, $P < 0.05$. Net assimilation rate was measured at PAR 2000 μmol m^{-2} s^{-1}, temperature 25°C, [H_2O vapor] ⩾18 mmol mol^{-1} air, [CO_2] 40 Pa, and flow rate 100 μmol m^{-2} s^{-1}. Stomatal conductance is the average rate of conductance measured during the entire A/C_i curve. Calculations of day respiration can be found in Appendix I.

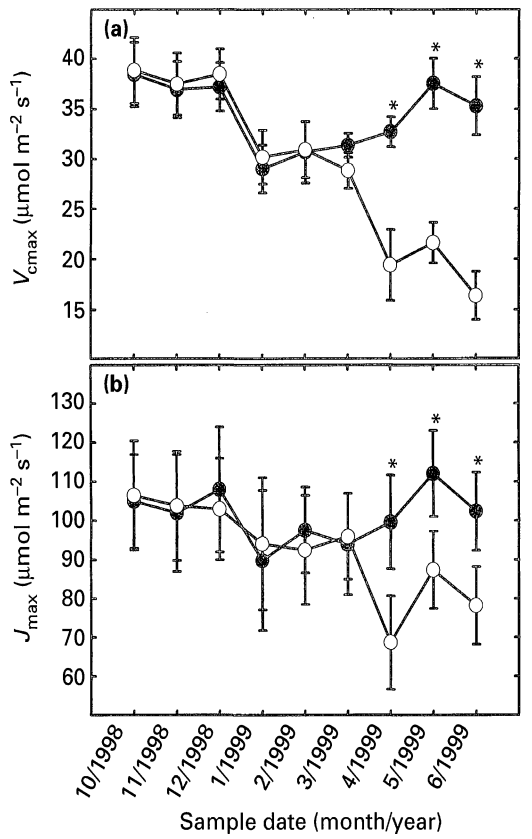

Fig. 2. Seasonal patterns of biochemical limitations to gas exchange in 2-yr-old Douglas-fir seedlings infected with *Paeocryptopus gaeumannii* (open circles, infected; closed circles, control). For each sample date, treatment differences were tested using a paired *t*-test; *, $P < 0.05$. Calculation of V_{cmax} and J_{max} can be found in Appendix I.

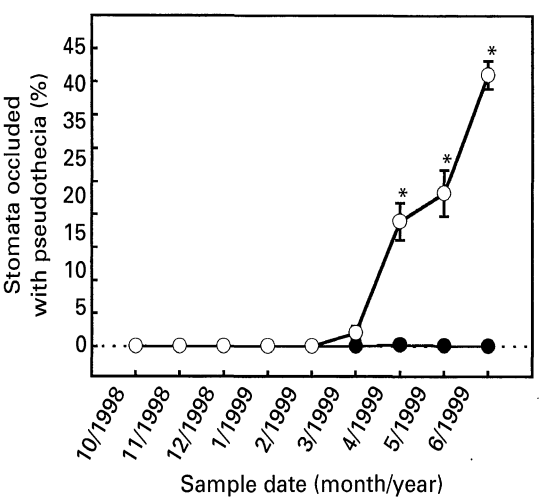

Fig. 3. Seasonal patterns of *Phaeocryptopus gaeumannii* infection in inoculated 2-yr-old Douglas-fir seedlings (open circles, infected; closed circles, control). For each sample date treatment differences were tested using a paired *t*-test; *, $P < 0.05$.

spring, which was also when stomatal conductance recovered. By May, V_{cmax} recovered to pre-winter values (e.g. V_{cmax} 37.55 (May) and 37.53 μmol CO_2 m^{-2} s^{-1} (Oct-Dec)). Similarly to Rubisco activation, RuBP regeneration (J_{max}) showed some seasonal changes, declining in the winter and recovering during the spring months (Fig. 2b).

The impact of fungal infection

Phaeocryptopus gaeumannii internal and external hyphal colonization and biomass increase gradually following inoculation (Capitano, 1999; D. Manter, unpublished); however, the first sign of physiological impact due to infection occurred 10 months after inoculation, or only after pseudothecia emerged from >5% of the needle stomata (i.e. March sample date; Figs 1–3). Reductions in net assimilation were associated with development of pseudothecia. For example, in April, when 18.9% of the stomata contained *P. gaeumannii* pseudothecia, net assimilation rates in ambient conditions (i.e. PAR *c.* 2000 μmol m^{-2} s^{-1}, [CO_2] 35.5 Pa, [H_2O vapor] *c.* 18 mmol

Table 1. *Infection level and* A/C_i *curve parameters from six 2-yr-old Douglas-fir seedlings infected with* Phaeocryptopus gaeumannii, *sampled in April 1999*

	Treatment[2]		
Parameter[1]	Control	Infected	*P*-value[3]
Pseudothecia count	0.23 (0.14)	18.91 (2.83)	0.001
Stomatal conductance	52.70 (9.32)	33.18 (5.02)	0.021
CO_2 assimilation rate	4.40 (0.36)	2.20 (0.24)	0.001
V_{cmax}	32.71 (3.55)	19.43 (1.52)	0.006
J_{max}	99.69 (12.13)	68.70 (11.78)	0.014
Day respiration	3.94 (0.76)	4.29 (0.30)	0.665

[1]Pseudothecia count, the percent of stomata occluded with pseudothecia (see the Materials and Methods section for further explanation). Stomatal conductance is the average value from the entire A/C_i curve measurement. CO_2 assimilation rates are single point measurements of assimilation at $[CO_2]$ *c.* 35.5 Pa, PAR *c.* 2000 μmol m^{-2} s^{-1}, $[H_20$ vapor] >18 mmol mol^{-1} air. V_{cmax}, J_{max}, and day respiration are derived from A/C_i curves as described in the text.
[2]One control and one infected branch from each of six 2-yr-old Douglas-fir seedlings were measured. Values reported are the mean and SE of the mean.
[3]*P*-values were calculated using paired *t*-tests between control and infected branched for the six seedlings sampled.

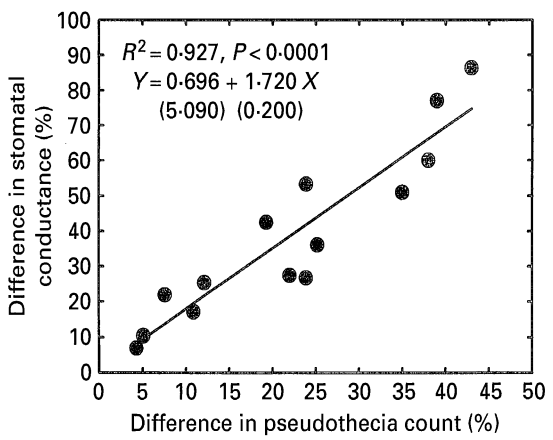

Fig. 4. Relationship between stomatal conductance and *Phaeocryptopus gaeumannii* pseudothecia in 2-yr-old Douglas-fir seedlings. Each observation represents differences between sample branches from each of the seedlings measured during the April–June sample dates. Percent decline in stomatal conductance = $(g_{sw\_control} - g_{sw\_infected})/g_{sw\_control} \times 100$. Percent difference in pseudothecia count = infected − control.

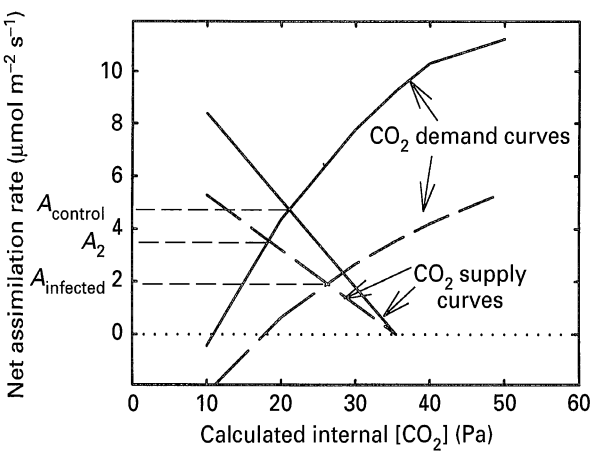

Fig. 5. Average A/C_i curves for control and *Phaeocryptopus gaeumannii*-infected branches in 2-yr-old Douglas-fir seedlings sampled in April 1999. Supply and demand curves were determined from the average values of V_{cmax}, J_{max}, R_{day} and conductance (Table 1) for each treatment (control, solid line; infected, dashed line) using the Eqns in Appendix I.

mol^{-1} air) declined by 50%, compared with control branches (Figs 1a, 3). Other physiological changes associated with the development of infection included a 37% reduction in stomatal conductance, a 40% reduction in Rubisco activation, and a 31% reduction in RuBP regeneration compared with control branches (Table 1).

No true control seedlings were used in our study, because branches adjacent to inoculated branches were covered with bags to obtain noninfected branches. It is possible that fungal growth on the infected branches influenced the physiology of the entire seedling via water stress, growth regulator, or source-sink relations. However, none of these factors appear to be associated with *P. gaeumannii* infection, and no 'compensatory' effect (e.g. an increase in net CO_2 assimilation rate) was observed in the control branches; all physiological parameters remained relatively constant throughout the study, except during the winter depression (Figs 1–3).

The relationship between fungal infection and stomatal conductance was determined by a regression between the percentage decline in stomatal conductance $(g_{sw,control} - g_{sw,infected}/g_{sw,control} \times 100)$ and pseudothecia presence (infected − control) using the observations from each seedling in April–June (Fig. 4). A strong positive, linear relationship between pseudothecia presence and the percentage decline in stomatal conductance was detected (adjusted $R^2 = 0.927$, $P < 0.0001$).

Fig. 5 depicts the average A/C_i or 'CO_2 demand' curve (calculated from the mean values of V_{cmax}, J_{max}

and R_{day} (from Table 1) in Eqn 2) and 'CO_2 supply' curve (calculated from the mean values of g_{sc} (from Table 1) in Eqn 4 when $C_a = 35$ Pa). The 'CO_2 demand' curve represents the response of photosynthesis to internal CO_2 concentration, demonstrating for the infected branches that photosynthesis is lower at all internal CO_2 concentrations. The 'CO_2 supply' curve depicts the amount of CO_2 entering the needle for a given stomatal conductance and atmospheric CO_2 concentration. The intersection of these two curves, or the point where the supply of CO_2 entering the needle through the stomata and the biochemical demand for CO_2 are equal, has been termed the 'operating point' and should approximate the realized rate of CO_2 assimilation at the designated C_a concentration (Jones, 1985). When this analysis is applied to the April measurements, predicted net assimilation rates (i.e. the 'operating point') at ambient CO_2 (35 Pa) are *c.* 4.7 and 1.9 μmol CO_2 m^{-2} s^{-1} for control and infected branches, respectively. These rates are similar to the measured rates of 4.4 and 2.2 μmol CO_2 m^{-2} s^{-1}, respectively (Table 1).

Changes in net CO_2 assimilation rates might occur through changes in either the CO_2 demand curve and/or the CO_2 supply curve. As shown in Fig. 5 both curves are affected by *P. gaeumannii* infection. If we assume that stomatal conductance and CO_2 supply affect infected needles first (see the Discussion section), followed by changes in Rubisco activation and CO_2 demand, then it appears that net CO_2 assimilation in infected needles is limited by approximately equal stomatal and biochemical limitations. For example, as stomatal conductance declines, the operating point shifts from $A_{control}$ to A_2, resulting in a *c.* 26% decline in net CO_2 assimilation. Next, as the demand curve changes, the operating point shifts from A_2 to $A_{infected}$, reducing net CO_2 assimilation by *c.* 34% or slightly more than half of the total decline in net ambient assimilation rate due to infection.

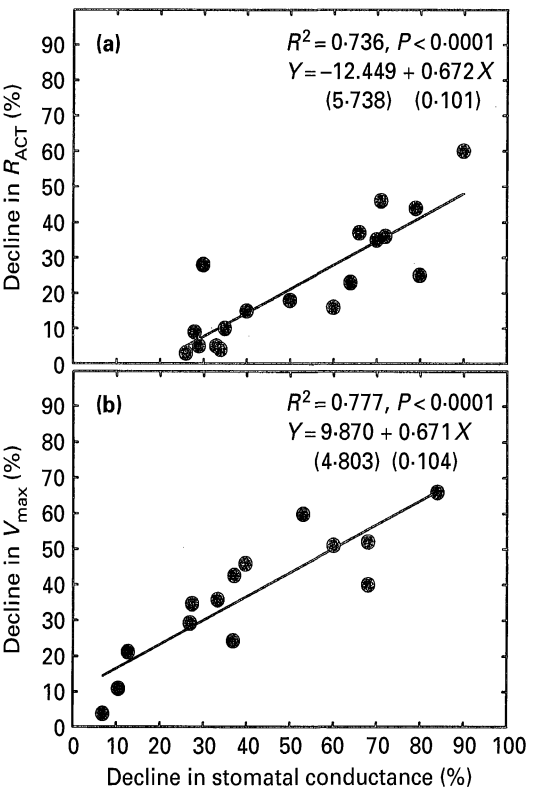

Fig. 6. Relationship between changes in stomatal conductance and Rubisco activation. (a) Determined from spectrophotometric analysis of Rubisco activation from needles treated with petroleum jelly. Each observation represents differences between treated needles from each of six seedlings measured in July 1999. Percent decline in Rubisco activation = $R_{ACT\_treatment\_0} - R_{ACT\_treatment\_i}$ (i, either the 50 or 100% treatment level). Percentage decline in stomatal conductance = $g_{sw\_treatment\_0} - g_{sw\_treatment\_i} / g_{sw\_treatment\_0} \times 100$ (i, either the 50 or 100% treatment level). Stomatal conductance was measured 1 h after treatment under ambient conditions. (b) Determined from A/C_i curve analysis of *P. gaeumannii*-infected seedlings. Each observation represents differences between control and infected branches. Percent decline in Rubisco activation = $V_{cmax\_control} - V_{cmax\_infected} / V_{cmax\_control} \times 100$. Percent decline in stomatal conductance = $g_{sw\_control} - g_{sw\_infected} / g_{sw\_control} \times 100$. Stomatal conductance is the average stomatal conductance measured during A/C_i curve analysis at optimal conditions.

Rubisco activation

Similarly to the A/C_i curve analysis, spectrophotometric assays of Rubisco activation also showed that branches infected with *P. gaeumannii* had a reduced amount of activated Rubisco compared with control branches (78.7±3.2 and 48.0±23.7% for the control and infected branches, respectively). However, no difference in the total Rubisco activity was detected (10.1±1.0 and 10.5±0.9 μmol m^{-2} s^{-1} for the control and infected branches, respectively).

Spectrophotometric assays of Rubisco activation using needles treated with petroleum jelly showed that Rubisco activation is lower in treated branches (i.e. lower stomatal conductance). In these seedlings, pre-treatment stomatal conductance did not significantly differ between branch samples (stomatal conductance was 142.7±9.07, 143.7±12.7 and 139.5±7.2 mmol m^{-2} s^{-1} for 0, 50 and 100% treatments, respectively); however, stomatal conductance was significantly reduced following treatment with petroleum jelly (stomatal conductance was 69.8±8.67, 48.86±7.4 and 27.92±4.5 mmol m^{-2} s^{-1} for 0, 50 and 100% treatments, respectively). The overall decline in stomatal conductance (e.g. *c.* 50% in controls) was associated with an increased vapor pressure deficit during the post-treatment measurements. A strong linear relationship (adjusted $R^2 = 0.736$, $P < 0.0001$) exists between the percentage decline in stomatal conductance following treatment ($g_{sw\_treatment\_0} - g_{sw\_treatment\_i} / g_{sw\_treatment\_0} \times 100$; i, either the 50 or 100% treatment level) versus the percentage decline in Rubisco activation ($R_{ACT\_treatment\_0} - R_{ACT\_treatment\_i}$; i, either the 50 or 100% treatment level) (Fig. 6a). A similar relationship between the percentage decline in stomatal

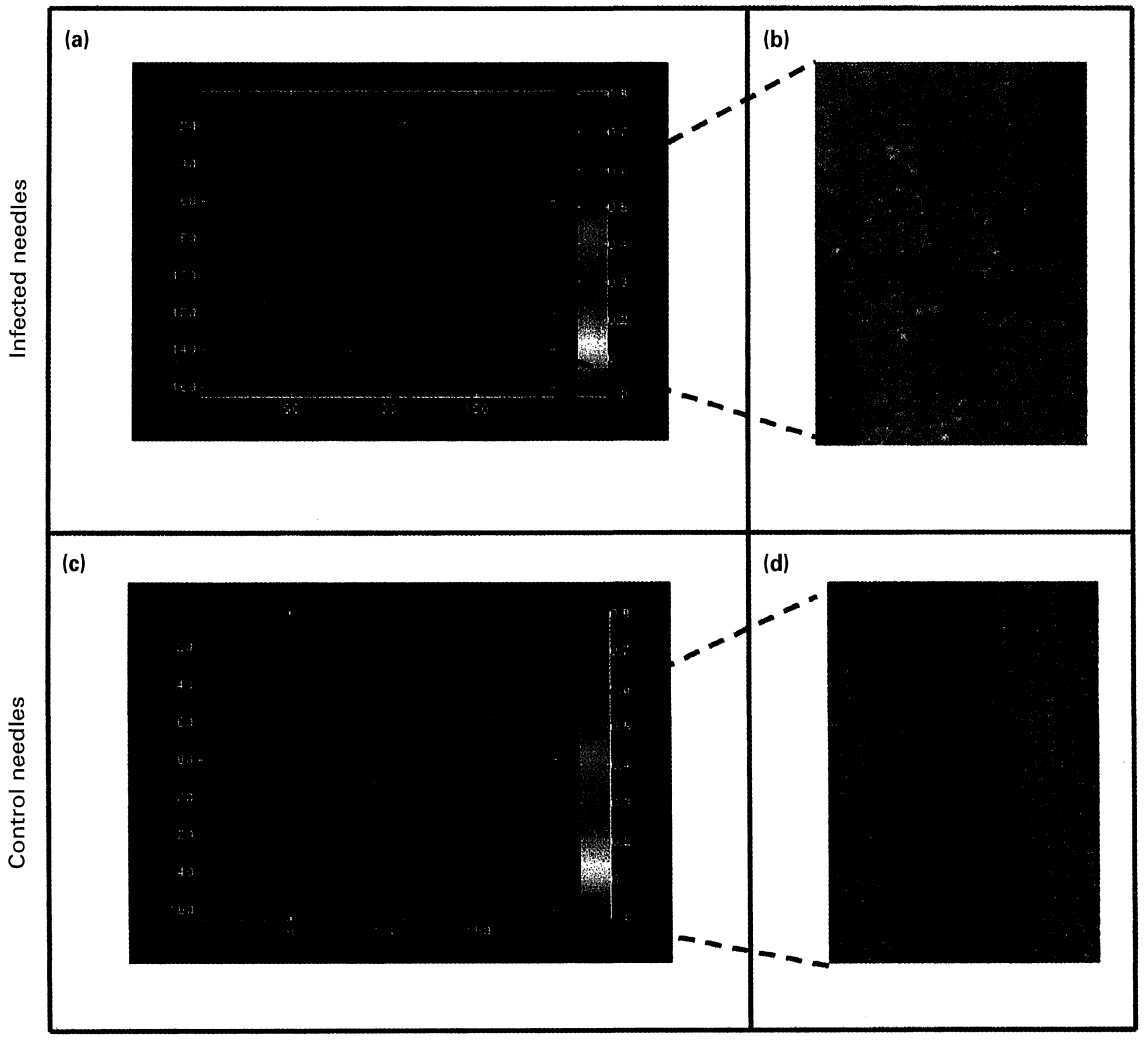

Fig. 7. Imaging chlorophyll fluorescence (Y') of 2-yr-old Douglas-fir seedlings infected with *Phaeocryptopus gaeumannii*. (a) and (c), images of chlorophyll fluorescence (Y'). (b) and (d), digital images showing the presence of pseudothecia from the region outlined in the adjacent panel.

conductance due to *P. gaeumannii* infection ($g_{sw\_control} - g_{sw\_infected}/g_{sw\_control} \times 100$) versus the percentage decline in Rubisco activation ($V_{cmax\_control} - V_{cmax\_infected}/V_{cmax\_control} \times 100$) was obtained using the A/C_i curve analysis of diseased seedlings ($R^2 = 0.777$, $P < 0.0001$; Fig. 6b).

Chlorophyll fluorescence

Chlorophyll fluorescence was measured to assess both quantum efficiency (Ning *et al.*, 1995; Bowyer *et al.*, 1998) and the presence of 'patchy' stomatal closure (Buckley *et al.*, 1997). Fig. 7 shows typical images of quantum efficiency (Y') from one control, and one infected, sample of needles from the same seedling. As can be seen in Fig. 7, no spatial variation in quantum efficiency can be observed within measured needles; thus, each set of needles measured had a quantum efficiency that showed a unimodal distribution of Y' values (data not shown).

No significant differences between needle segments were detected (i.e. tip and petiole halves, data not shown) therefore; the average value of the tip and petiole halves for each branch-treatment combination was used for subsequent analyses. No difference in quantum efficiency was detected between control and infected branches from the same seedling (0.693 ± 0.014 and 0.686 ± 0.014 for the control and infected branches, respectively). In addition, no differences were detected in F_m, F_s or F_{dark} (data not shown).

DISCUSSION

Seasonal variation

Seasonal changes in needle physiology (i.e. gas exchange) were observed for both infected and control branches of 2-yr-old Douglas-fir seedlings. However, no difference between infected and non-infected branches was noted until there were obvious pseudothecia present in infected needles. Depressions of needle physiology during the winter are a typical phenomenon in conifers, particularly at higher elevations (Havranek & Tranquillini, 1995). In our work, winter depressions of Douglas-fir needle physiology have been detected in seedlings (present study) and saplings, *c.* 15-yr-old (K.

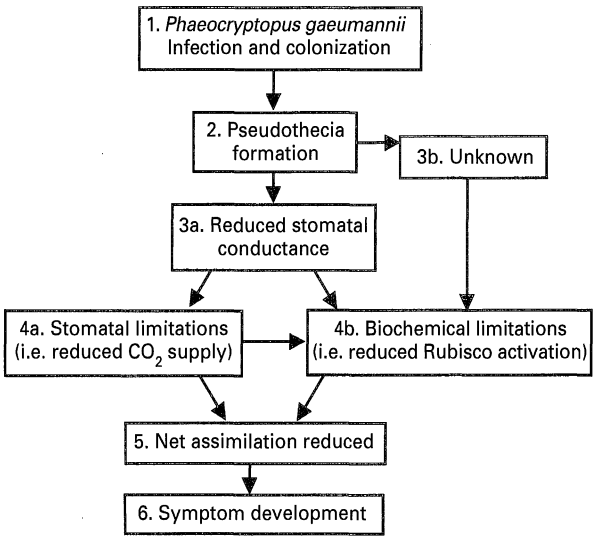

Fig. 8. Mechanism of *Phaeocryptopus gaeumannii* impact on Douglas-fir needle physiology (gas exchange).

Kavanagh, unpublished). Although the causes of these depressions were not directly investigated, other work with conifers suggests that increased levels of abscisic acid (Qamaruddin *et al.*, 1993) might be one of the factors responsible for the increased stomatal closure and decline in conductance. Similarly to the disease mechanism to be presented, the reduced supply of CO_2 from the low stomatal conductance might cause a down-regulation in the activation of Rubisco. However, 'normal seasonal changes in cell physiology' (Havranek & Tranquillini, 1995) such as membrane permeability should not be overlooked.

Fungal impacts and mechanism

Following pseudothecia emergence, both stomatal conductance and C assimilation are reduced in infected branches.

Based on this study we propose the following mechanism through which *P. gaeumannii* affects Douglas-fir needle physiology and potential productivity (Fig. 8). Most fungal effects result from the formation of pseudothecia, a resultant decline in stomatal conductance and the development of stomatal and nonstomatal limitations to CO_2 assimilation (steps 1–5). Additional nonstomatal limitations to CO_2 assimilation might also arise from an as yet undetermined fungal effect (step 3b). Once assimilation rates have been reduced, needles will be less productive and over time the common SNC disease symptoms of chlorosis, needle abscission, and growth loss will result (step 6).

In our model, the major impact of disease occurs with the emergence of fungal pseudothecia. At this point, stomatal conductance and net CO_2 assimilation are reduced. Understanding the mechanisms responsible for the changes in either one of these parameters is complicated by the fact that each has been shown to influence the other. It is our contention, however, that a decrease in stomatal conductance (and increased stomatal limitation to net CO_2 assimilation) occurs first owing to the formation of pseudothecia, followed by an increase in biochemical limitations to net CO_2 assimilation because of reduced Rubisco activation.

A direct effect of pseudothecia on stomatal conductance is expected because of the physical presence of pseudothecia in needle stomata. Furthermore, the strong relationship between pseudothecia presence and decline in stomatal conductance suggests that the presence of pseudothecia is the causal factor reducing stomatal conductance in SNC-infected Douglas-fir foliage. If the relationship presented in Fig. 4 is extrapolated to zero stomatal conductance (i.e. 100% decline in stomatal conductance), then only *c.* 58% of the stomata need be occupied by pseudothecia. This might be owing to the presence of other fungal structures that also block gas exchange through needle stomata. One structure, pseudothecia initials (i.e. generative hyphae), might prove to be the best indicator of fungal impact on stomatal conductance, because these structures can be found densely packed into needle stomata with or without attached mature pseudothecia (Stone & Carroll, 1986). Second, surface hyphae in *P. gaeumannii*-infected foliage can at times form relatively dense mats of hyphae on the needle surface (Capitano, 1999) and these structures might also physically block needle gas exchange, as has been shown with powdery mildew (Ayres, 1976, 1981).

Concurrent with the decline in stomatal conductance, net CO_2 assimilation is reduced through both stomatal and biochemical means. We suggest that the biochemical limitations, due to Rubisco deactivation, result from the reduced stomatal conductance and internal CO_2 concentration. In other studies, the amount of activated Rubisco was affected by other factors, such as water stress (Kanechi *et al.*, 1996; Tezara *et al.*, 1999), feedback inhibition (Scholes, 1992), nitrogen (N) concentration (Farquhar *et al.*, 1980) and fungal toxins (Scholes, 1992). However, if any of these factors were limiting Rubisco activation in *P. gaeumannii*-infected needles, then we would have expected them to be present during the long infection period before pseudothecia formation. Instead our research shows that reduced Rubisco activation due to fungal presence occurred only after pseudothecia formation. Furthermore, any fungal consumption of key nutrients such as N does not appear to be related to the decline in Rubisco activation as no change in total Rubisco activity (R_T) was detected in infected branches.

Two possible mechanisms might explain the relationship between stomatal conductance and Rubisco activation. The first potential mechanism involves what is commonly referred to as 'patchy' stomatal closure (Terashima *et al.*, 1988; Terashima,

1992; Mott, 1995). In this situation, stomata are closed in groups, resulting in a needle-wide conductance distribution that has distinct modes; typically, it is bimodal with one region possessing a normal conductance and the other little to no conductance (Buckley *et al.*, 1997). If such a distribution is present, A/C_i curve analysis might erroneously show nonstomatal limitations owing to an overestimate of C_i (Terrashima *et al.*, 1988).

In the case of *P. gaeumannii*-infected foliage, however, patchy stomatal closure does not appear to be responsible for our observed biochemical limitations to assimilation. First, spectrophotometric assays of Rubisco activation, which do not rely on estimates of C_i, confirmed that Rubisco activation is reduced in infected needles. Second, chlorophyll fluorescence images show that quantum efficiency, in both infected and control needles, conforms to a unimodal distribution.

The second possible mechanism is that the reduction in CO_2 supply due to lower stomatal conductance results in a reduction in the amount of activated Rubisco. For Rubisco to act as a carboxylase and fix C, it must first be activated. One of the steps in activation involves carbamylation of the active site with a CO_2 molecule (Lorimer, 1981). Therefore, following the decline in stomatal conductance, and a reduction in the supply of internal CO_2, it is possible that the amount of activated Rubisco declines, resulting in our observed reductions in V_{cmax}. In order to test the sensitivity of Rubisco activation in Douglas fir to internal [CO_2], we measured Rubisco activation from healthy needles that had an artificially reduced stomatal conductance. Based on these studies, Rubisco activation in Douglas-fir needles is influenced by decreasing stomatal conductance and the resulting decline in internal CO_2 concentration. In fact, Rubisco activation showed a linear relationship with maximal stomatal conductance, decreasing as stomatal conductance decreased. To our knowledge, a linear relationship between maximum stomatal conductance (and the associated decline in internal CO_2 concentration) and Rubisco activation has not previously been shown. However, Rubisco activation has been shown to decline below some threshold level of internal CO_2, which varies between species (von Caemmerer & Edmondson, 1986; Sage *et al.*, 1990).

Reductions in Rubisco activation in *P. gaeumannii*-infected foliage also appear to arise directly from the decline in internal [CO_2], for the following reasons. First, biochemical limitations to net assimilation were consistently associated with changes in stomatal conductance (i.e. *P. gaeumannii*-infected seedlings, petroleum-jelly-treated seedlings, and winter-associated physiological depressions). Second, no changes in any of the chlorophyll-fluorescence parameters were detected following fungal infection. From these data we can infer that *P. gaeumannii* infection appears to have no direct impact on the level and function of energy capture and electron transfer, or any of the other physiological processes typically associated with changes in chlorophyll fluorescence (Kraus & Weis, 1991). Third, physical reductions in stomatal conductance (i.e. petroleum-jelly-treated needles) of healthy needles resulted in reduced Rubisco activation. Fourth, no differences in total Rubisco activity were detected.

Reduced stomatal conductance and CO_2 supply might not fully account for the changes in Rubisco activation of *P. gaeumannii*-infected needles (Fig. 6a,b). For example, in the petroleum-jelly-treated trees, when stomatal conductance declined by 50%, Rubisco activation was reduced by *c.* 21%; however, in SNC-infected seedlings, when fungal presence caused a 50% reduction in stomatal conductance, Rubisco activation was reduced by *c.* 43%. Assuming that the observed differences are not related to the differing methodologies (spectrophotometric vs A/C_i curve determination of Rubisco activation), then only *c.* 50% of the nonstomatal limitations in *P. gaeumannii*-infected foliage can be attributed to the stomatal conductance mechanism already explained. The increased sensitivity to stomatal conductance and internal CO_2 supply in *P. gaeumannii*-infected needles, if it is present, deserves further attention.

Finally, only after the decline in net assimilation occurs do we reach the final stage of disease development, or symptom expression. During this stage, the commonly observed patterns of chlorosis, needle abscission and reduced growth develop in *P. gaeumannii*-infected foliage.

ACKNOWLEDGEMENTS

The work presented here was funded by the Swiss Needle Cast Cooperative, Oregon State University, Corvallis, OR, USA. The authors wish to thank Dr Larry S. Daley and Li Ping for kindly providing us with instruction and use of their imaging chlorophyll fluorometer; and Dr Lailiang Cheng and Guillaume Gruere for assistance with the spectrophotometric Rubisco assays. We are also grateful to Dr Jeffrey Stone for review and helpful discussions.

REFERENCES

Ayres PG. 1976. Patterns of stomatal behaviour, transpiration and CO_2 exchange in pea following infection by powdery mildew (*Erysiphe pisi*). *Journal of Experimental Botany* **27**: 1196–1205.

Ayres PG. 1981. Effects of disease on plant water relations. In: Ayres PG, ed. *Effects of disease on the physiology of the growing plant*. Cambridge, UK: Cambridge University Press, 131–148.

Bowyer WJ, Ning L, Daley LS, Strobel GA, Edwards GE, Callis JB. 1998. *In vivo* fluorescence imaging for detection of damage to leaves by fungal phytotoxins. *Spectroscopy* **13**: 36–44.

Buckley TN, Farquhar GD, Mott KA. 1997. Qualitative effects of patchy stomatal conductance distribution features on gas-exchange calculations. *Plant, Cell & Environment* **20**: 867–880.

Capitano B. 1999. *The infection and colonization of Douglas-fir by* P. gaeumannii. MSc thesis, Oregon State University, Corvallis, OR, USA.

Ehlringer J, Pearcy RW. 1983. Variation in quantum yield for CO_2 uptake among C_3 and C_4 plants. *Plant Physiology* **73**: 555–559.

Farquhar GD, von Caemmerer S, Berry JA. 1980. A biochemical model of photosynthetic CO_2 assimilation in leaves of C_3 species. *Planta* **149**: 78–90.

Gordon TR, Duniway JM. 1982. Effects of powdery mildew infection on the efficiency of CO_2 function and light utilization by sugar beet leaves. *Plant Physiology* **69**: 139–142.

Hansen EM, Stone JK, Capitano BR, Rosso P, Sutton W, Winton L, Kanaskie A, McWilliams MG. 2000. Incidence and impacts of Swiss needle cast in forest plantations of Douglas-fir in Coastal Oregon. *Plant Disease* **84**: 773–778.

Harley PC, Sharkey TD. 1991. An improved model of C_3 photosynthesis at high CO_2: reversed O_2 sensitivity explained by lack of glycerate re-entry into the chloroplast. *Photosynthesis Research* **27**: 169–178.

Harley PC, Thomas RB, Reynolds JF, Strain BR. 1992. Modeling photosynthesis of cotton grown in elevated CO_2. *Plant, Cell & Environment* **15**: 271–282.

Havranek WA, Tranquillini W. 1995. Physiological processes during winter dormancy and their ecological significance. In: Smith WK, Hinckley TM, eds. *Ecophysiology of coniferous forests*. New York, USA: Academic Press, 95–124.

Jones HG. 1985. Partitioning stomatal and non-stomatal limitations to photosynthesis. *Plant, Cell & Environment* **6**: 671–674.

Kanechi M, Uchida N, Yasuda T, Yamaguchi T. 1996. Non-stomatal inhibition associated with inactivation of rubisco in dehydrated coffee leaves under unshaded and shaded conditions. *Plant and Cell Physiology* **37**: 455–460.

Kraus GH, Weis E. 1991. Chlorophyll fluorescence and photosynthesis: the basics. *Annual Review of Plant Physiology and Plant Molecular Biology* **42**: 313–349.

Lorimer GH. 1981. The carboxylation and oxygenation of ribulose 1,5-bisphosphate: the primary events in photosynthesis and photorespiration. *Annual Review of Plant Physiology* **32**: 349–383.

Montalbini P, Buchanan BB, Hutcheson SW. 1981. Effect of rust infection on rates of photochemical polyphenol oxidase activity of *Vicia faba* chloroplast membranes. *Physiological Plant Pathology* **18**: 51–57.

Mott KA. 1995. Effects of patchy stomatal closure on gas exchange measurements following abscisic acid treatment. *Plant, Cell & Environment* **18**: 1291–1300.

Ning L, Edwards GE, Strobel GA, Daley LS, Callis JB. 1995. Imaging fluorometer to detect pathological and physiological change in plants. *Applied Spectroscopy* **49**: 1381–1389.

Qamaruddin M, Dormling I, Ekberg I, Eriksson G, Tillberg E. 1993. Abscisic acid content at defined levels of bud dormancy and frost tolerance in two contrasting populations of *Picea abies* grown in a phytotron. *Plant Physiology* **87**: 203–210.

Sage RG, Sharkey TD, Seemann JR. 1990. Regulation of rubulose-1,5-bisphosphate carboxylase activity in response to light intensity and CO_2 in the C_3 annuals *Chenopodium album* L. and *Phaseolus vulgaris* L. *Plant Physiology* **94**: 1735–1742.

Scholes JD. 1992. Photosynthesis: cellular and tissue aspects in diseased leaves. In: Ayres PG, ed. *Pests and pathogens*. Oxford, UK: Bios Scientific Publishers, 85–106.

Sharkey TD. 1985. Photosynthesis in intact leaves of C_3 plants: physics, physiology and rate limitations. *The Botanical Review* **51**: 53–105.

Stone JK, Carroll GC. 1986. Observations on the development of ascocarps of *Phaeocryptopus gaeumannii* and on the possible existence of an anamorphic state. *Sydowia* **38**: 317–323.

Šutić DD, Sinclair JB. 1991. *Anatomy and physiology of diseased plants*. Boca Raton, FL, USA: CRC Press.

Tang X, Rolfe SA, Scholes JD. 1992. The effect of *Albugo candida* (white blister rust) on the photosynthetic and carbohydrate metabolism of leaves of *Arabidopsis thaliana*. *Plant, Cell & Environment* **19**: 967–975.

Terashima I. 1992. Anatomy of non-uniform leaf photosynthesis. *Photosynthesis Research* **31**: 195–212.

Terashima I, Wong S-C, Osmond CB, Farquhar GD. 1988. Characterization of non-uniform photosynthesis induced by abscisic acid in leaves having different mesophyll anatomies. *Plant and Cell Physiology* **29**: 385–394.

Tezara W, Mitchell VJ, Driscoll SD, Lawlor DW. 1999. Water stress inhibits plant photosynthesis by decreasing coupling factor and ATP. *Nature* **401**: 914–917.

von Caemmerer S, Edmondson DL. 1986. Relationship between steady-state gas exchange, *in vivo* ribulose bisphosphate carboxylase activity and some carbon reduction cycle intermediates in *Raphanus sativus*. *Australian Journal of Plant Physiology* **13**: 669–688.

Walters D, Ayres PG. 1984. Ribulose bisphosphate carboxylase protein and enzymes of CO_2 assimilation in barley infected by powdery mildew (*Erysiphe graminis hordei*). *Phytopathologische Zeitschrift* **109**: 208–218.

Wullschleger SD. 1993. Biochemical limitations to carbon assimilation in C_3 plants – a retrospective analysis of the A/C_i curves from 109 species. *Journal of Experimental Botany* **44**: 907–920.

APPENDIX I. A/C_i *curve analysis and calculations*

A/C_i curves can be used to estimate some of the major underlying biochemical processes influencing gas exchange and the net uptake of C into a plant (assimilation) (Farquhar *et al.*, 1980; Sharkey, 1985; Harley & Sharkey, 1991; Harley *et al.*, 1992). According to their models, CO_2 assimilation (μmol m^{-2} s^{-1}) can be modeled by Eqns 1 and 2. See Appendix II for variable definitions.

$$A = V_c - 0.5V_o - R_{day} \quad \text{Eqn 1}$$

$$A = (1 - 0.5\frac{O}{\tau \times C_i}) \times \min\{W_c, W_j, W_p\} - R_{day} \quad \text{Eqn 2}$$

$$\tau = \exp(-3.9489 + 28.9/0.00831 \times T_k) \quad \text{Eqn 3}$$

Implicit in Eqn 1 is that for each carboxylation event one molecule of CO_2 is assimilated, and for every two oxygenations one CO_2 molecule is released. C_i is the calculated internal [CO_2] (Pa) based on Eqns 4–6.

$$A = g_{sc}(C_a - C_i) \quad \text{Eqn 4}$$

$$E = g_{sw}(W_a - W_i) \quad \text{Eqn 5}$$

$$g_{sc} = \frac{g_{sw}}{160} \quad \text{Eqn 6}$$

Furthermore, according to Farquhar *et al.* (1980) if Rubisco assumes Michaelis-Menton enzyme kinetics based on a competitive two-substrate (O_2 and CO_2) system, then:

$$W_c = \frac{V_{c\max} \times C_i}{C_i + K_c(1 + \frac{O}{K_o})} \quad \text{Eqn 6}$$

$$K_c = \exp(35.79 - 80.47/0.00831 \times T_k) \quad \text{Eqn 7}$$

$$K_o = \exp(9.59 - 14.51/0.00831 \times T_k) \quad \text{Eqn 8}$$

and

$$W_j = \frac{\mathcal{J} \times C_i}{4(C_i + \frac{O}{\tau})} \quad \text{Eqn 9}$$

assuming that for every 4 electrons produced enough ATP and NADPH are generated for completion of

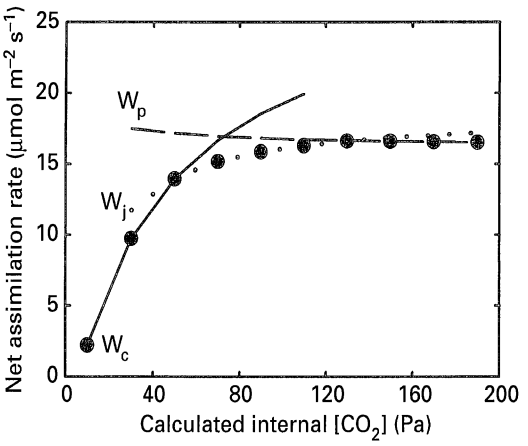

Fig. 9. The components of an A/C_i curve. Closed circles, a typical A/C_i curve consisting of three underlying biochemical processes: W_c, rate of caroxylation limited by Rubisco activation; W_j, rate of carboxylation limited by RuBP regeneration; W_p, rate of carboxylation limited by inorganic phosphate.

the Calvin cycle and regeneration of RuBP. The potential rate of electron transport is dependent upon the following:

$$\mathcal{J} = \frac{\alpha \times I}{(1+\frac{\alpha^2 I^2}{\mathcal{J}_{max}{}^2})^{0.5}} \qquad \text{Eqn 10}$$

Quantum-use efficiency (α) was assumed to be 0.18 (mol e^- mol^{-1} absorbed photons) for both control and inoculated branches; Ehlringer & Pearcy (1983) showed that quantum-use efficiency and light absorption is relatively constant among several C_3 plants; and,

$$W_p = 3 \times TPU + \frac{V_o}{2} = 3 \times TPU + \frac{V_c \times 0.5 \times O}{C_i \times \tau} \qquad \text{Eqn 11}$$

Finally, Eqn (2) was solved iteratively for V_{max} and R_{day} by assuming that W_c occurs at low C_i values. Wullschleger (1993) suggests using the portion of the curve where C_i <30 Pa; however when V_{cmax} values are low, the best fit might be obtained using larger portions of the curve (e.g. C_i <50 Pa). Therefore, for each curve the largest range of C_i values that produced the best fit to the W_c form of Eqn 2 was used to determine V_{cmax} and R_{day}. After determining V_{max} and R_{day}, $\mathcal{J}_{max}$ and the rate of phosphate release in triose phosphate utilization (TPU) were determined by solving the entire A/C_i response curve for the full version of Eqn 2 (Fig. 9).

APPENDIX II. *Abbreviations and units*

Abbreviation	Parameter	Units
A	Assimilation rate	μmol m^{-2} s^{-1}
C_a	Atmospheric CO_2 concentration	35.5 Pa
C_i	Internal CO_2 concentration	Pa
E	Transpiration rate	mmol m^{-2} s^{-1}
F_m	Maximal fluorescence	Not applicable
F_s	Steady-state fluorescence at 150 s	Not applicable
F_{dark}	Machine background fluorescence	Not applicable
g_{sc}	Stomatal conductance to CO_2	mmol m^{-2} s^{-1}
g_{sw}	Stomatal conductance to H_2O	mmol m^{-2} s^{-1}
I	Incident light	μmol m^{-2} s^{-1}
$\mathcal{J}$	Potential rate of electron transport	μmol m^{-2} s^{-1}
$\mathcal{J}_{max}$	Light saturated rate of electron transport	μmol m^{-2} s^{-1}
K_c	Michaelis-Menton constants for CO_2	Pa
K_o	Michaelis-Menton constants for O_2	KPa
O	Internal oxygen concentration	21 kPa
R_{ACT}	Rubisco activation, $R_I/R_T \times 100$	%
R_{day}	Evolution of nonphotorespiratory CO_2 in light	μmol m^{-2} s^{-1}
R_I	Initial Rubisco activity	μmol m^{-2} s^{-1}
R_T	Total Rubisco activity	μmol m^{-2} s^{-1}
τ	Specificity of Rubisco for O_2/CO_2	μmol m^{-2} s^{-1}
TPU	Rate of phosphate release in triose phosphate utilization	μmol m^{-2} s^{-1}
V_c	Rubisco carboxylation	μmol m^{-2} s^{-1}
V_o	Rubisco oxygenation	μmol m^{-2} s^{-1}
V_{cmax}	Rubisco activation	μmol m^{-2} s^{-1}
W_a	Vapor pressure of the air	mmol H_2O mol^{-1} air
W_c	Rate of carboxylation limited by Rubisco activation	μmol m^{-2} s^{-1}
W_i	Internal leaf vapor pressure	mmol H_2O mol^{-1} air
W_j	Rate of carboxylation limited by RuBP regeneration	μmol m^{-2} s^{-1}
W_p	Rate of carboxylation limited by inorganic phosphate	μmol m^{-2} s^{-1}
Y'	Quantum efficiency, $(F_m-F_s)/(F_m-F_{dark})$	Not applicable